INTERLAYER EXCHANGE COUPLING
ACROSS EPITAXIAL Si SPACERS

D. E. BÜRGLER, R. R. GAREEV, L. L. POHLMANN, H. BRAAK, M. BUCHMEIER,
M. LUYSBERG, R. SCHREIBER, AND P. A. GRÜNBERG

Institut für Festkörperforschung, Forschungszentrum Jülich GmbH

D-52425 Jülich, Germany

Abstract: We report on sizable antiferromagnetic interlayer exchange coupling (AFC) of Fe(001) layers across epitaxial Si spacers, for which epitaxial growth of a pseudomorphic phase stabilized by the interface is confirmed by low-energy electron diffraction and high-resolution transmission electron microscopy. The coupling strength decays with spacer thickness on a length scale of a few Å and shows a negative temperature coefficient. Transport measurements of lithographically structured junctions in current-perpendicular-to-plane geometry show the validity of the three "Rowell criteria" for tunneling: (i) exponential increase of resistance R with thickness of the barrier, (ii) parabolic dI/dV-V curves, and (iii) slight decrease of R with increasing temperature. Therefore, AFC is mediated by non-conductive spacers, which in transport experiments act as tunneling barriers with a barrier height of several tenths of an eV. We discuss our data, in particular the strength, thickness and temperature dependence, in the context of two previously proposed models for AFC across non-conducting spacers. We find that neither the molecular-orbital model for heat-induced effective exchange coupling nor the quantum interference model extended to insulator spacers by introducing complex Fermi surfaces can account for the strong AFC across epitaxial Si spacers.

1. INTRODUCTION

Magnetic interlayer exchange coupling across metallic spacer layers was discovered in 1986 by Grünberg *et al.* [1] and has been extensively investigated. It is well established that the coupling displays a damped oscillation between the ferro- and antiferromagnetic (AF) state as a function of the interlayer thickness [2]. The AF coupling strengths at the first coupling maximum are typically of the order of 1 mJ/m². Theoretically, it was shown that the coupling across metals is due to the formation of standing electron waves in the interlayer, which result from spin-dependent electron interface reflectivity. When applying the same theoretical framework to insulating or semiconducting interlayers, however, Bloch states in the spacer have to be replaced by evanescent states, which exponentially decay with distance from the interfaces to the metallic, magnetic layers [3]. Accordingly, the coupling strength is also expected to exponentially decay when the thickness of a non-conducting interlayer increases. Furthermore, this model predicts an increase of the coupling strength with temperature for insulating spacers [3, 4] in clear contrast to metallic interlayers, where the model predicts and experiments confirm a decreasing coupling strength with temperature. The experimental data basis concerning coupling across non-metallic spacers is rather thin. For amorphous insulators like a-SiO₂ and a-Al₂O₃, which are widely employed *e.g.* in tunneling magneto-resistance devices, interlayer exchange coupling is not observed experimentally. However, there is a recent report of AF coupling with a strength of about 0.26 mJ/m² in epitaxial Fe/MgO/Fe(100) structures for very thin (<7 Å) MgO thicknesses [5]. This report and our observation of even stronger

antiferromagnetic interlayer exchange coupling (AFC) across nominally pure Si [6] focuses particular interest on this new class of highly resistive structures exhibiting non-oscillatory AFC.

Previously, we have found that insulating-type, highly resistive Si spacers can be prepared by a certain deposition procedure [6-8]. Corresponding Fe/Si/Fe structures reveal very strong AFC with a total coupling strength in excess of 5 mJ/m^2 [6], which could be further increased to 8 mJ/m^2 by inserting thin epitaxial and metallic FeSi boundary layers at interfaces [8]. The just mentioned coupling strengths are among the strongest reported in literature including metallic spacers [2] and exceed the values obtained for metallic $Fe_{0.5}Si_{0.5}$ spacers grown by co-evaporation by one order of magnitude [7]. The thickness dependence of the coupling is oscillatory for metallic $Fe_{0.5}Si_{0.5}$ spacers, but exponentially decaying for Si-rich, highly resistive spacers. For combined semiconducting/metallic epitaxial spacers (*i.e.* nominally pure Si/$Fe_{0.5}Si_{0.5}$), the main impact to AFC originates from the semiconducting part of the spacer [9]. Finally, we also reported sizable AFC across epitaxial, Ge-containing spacers, when direct contact between Ge and Fe is prevented, *e.g.* by inserting thin Si boundary layers or by piling up thin layers of Ge and Si to form Si-Ge-multilayers [10]. The latter results indicate that relatively strong AFC might be a common feature of well-ordered, epitaxial semiconducting spacer layers.

In order to clarify the coupling mechanism and to perform meaningful *ab-initio* calculations, detailed knowledge about the spacer layer in terms of structure as well as electronic properties is needed. High-resolution transmission electron microscopy (TEM) images as well as low-energy electron diffraction (LEED) are employed to study the crystalline structure of the Si interlayers, and we perform transport measurements with the current flowing per-pendicular to the samples plane (CPP) to obtain additional and clear information whether Si-rich spacers are metallic or insulating. A further question is whether the transport in highly resistive spacers is due to elastic tunneling, or whether it arises from additional channels of conductivity across submicron-sized pinholes, as it was pointed out in Refs. [11, 12]. Pinholes also provide contacts between the FM layers where direct exchange interaction could strongly influence the coupling behavior. In fact, this extrinsic pinhole-induced coupling could obscure the intrinsic coupling mechanism. In order to address these questions we examine for epitaxial Fe/Si/Fe structures the validity of the necessary and sufficient Rowell criteria for direct elastic tunneling [12], *i.e.* (i) strong and exponential increase of the resistance R with spacer thickness t, (ii) parabolic dependence of conductivity *versus* bias voltage, and – most decisive – (iii) small and negative temperature coefficient of the zero-bias resistance [13]. Additionally, we measure the temperature dependence of the coupling as a further characteristic that can be compared to theoretical predictions for AFC across non-metallic spacers as presented in the concluding discussion.

2. EXPERIMENTAL PROCEDURES

2.1. Sample preparation

We grow our Fe/Si/Fe(001) structures in a molecular-beam epitaxy system using a 150 nm-thick Ag(001) buffer system on GaAs(001) [6, 7]. The layers forming the spacers are deposited at low deposition rates (< 0.1 Å/s) and at room temperature (RT). In some cases the spacers are grown in the shape of wedges to facilitate the study of thickness dependences. The nominal thickness of the wedges ranges from 8 to 20 Å over a lateral distance of typically 10 mm, and the Fe layer thicknesses lie in the range between 50 and 100 Å.

2.2 Magnetic and structural characterization

Magnetic properties are measured by magneto-optical Kerr effect (MOKE) in Voigt geometry, by magnetometry using a superconducting quantum interference device (SQUID), and Brillouin light scattering from spin waves (BLS). Bilinear (J_1) and biquadratic (J_2) coupling constants are determined by fitting the field dependence of MOKE, SQUID, and BLS data using the standard areal energy density expression

$$E_{ex} = -J_1 \cos(\Theta) - J_2 \cos^2(\Theta) \tag{1}$$

to phenomenologically describe interlayer exchange coupling, where Θ is the angle between the two Fe film magnetizations. The external magnetic field for all three techniques is applied along an easy-axis of Fe(001) in the plane of the sample. Further details concerning the preparation of the structures, their characterization, and the fitting procedures are described in Refs. [6, 7, 14].

The in-plane crystalline structure of all layers is characterized by means of *in-situ* LEED measurements. A TEM with aberration correction [15] is employed to obtain high-resolution images of Si spacer layers.

2.3. Lithography and transport measurements

The CPP transport measurements are performed after patterning 10×10 mm^2-sized, wedge-type samples using photolithography, ion-beam etching, and the lift-off technique. The layout of the patterned sample is shown in Fig. 5(a). In this way we obtain CPP junctions with different Si spacer thicknesses t and variable junction areas A, which all are deposited under the same growth conditions. We use crossed contacts, where a 300 nm-thick Cu layer forms the upper electrode. The patterned 150 nm-thick silver buffer layer serves as a bottom electrode. The sheet resistances of both electrodes are about 0.1 Ω and thus significantly smaller than the resistance of the tunneling junctions in CPP geometry (5-300 Ω), such that current distribution effects are diminished [16]. Insulation of the electrodes is achieved by deposition of a 250 nm-thick Si-oxide layer. Finally, we define junctions of rectangular shape ranging in area A from 22 to more than 200 μm^2. A photograph of a typical junction is shown in the inset of Fig. 5(a). After patterning, voltage and current leads suitable for four-point transport measurements are connected by ultrasonic bonding to measure the *I-V* characteristics of the junctions.

3. RESULTS

3.1. Structural characterization

Examples of LEED patterns of a 5 nm-thick bottom Fe(001) layer and a 5 Å-thick Si interlayer grown on the top of the bottom Fe layer are shown in Fig. 1. Both patterns are taken at an electron energy of 55 eV and reveal the same surface reciprocal lattice in terms of symmetry, relative orientation, and lattice constants. The superimposed dashed lines connect the (01) spots and yield an in-plane lattice constant of 2.9 Å, the bulk value of bcc-Fe. Therefore, the in-plane structure of thin Si layers is the same as for the Fe(001) surface. The LEED pattern of the top Fe(001) layer (not shown), *i.e.* the 5 to 10 nm-thick Fe layer grown on top of the Si spacer of Fig. 1(b), is very similar to the one of the bottom Fe layer shown in Fig. 1(a) and confirms the epitaxial growth throughout the whole stack.
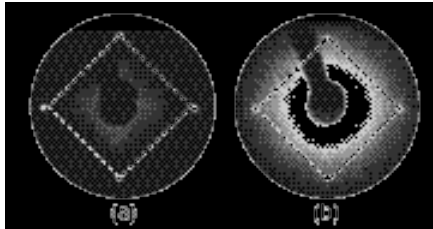

Fig. 1. LEED patterns of a 5 nm-thick Fe(100) bottom layer (a) and a 5 Å-thick Si spacer (b) grown at RT on the Fe layer shown in (a). Dashed lines mark the in-plane reciprocal lattice of bulk bcc-Fe(001) corresponding to an in-plane lattice constant of 2.9 Å
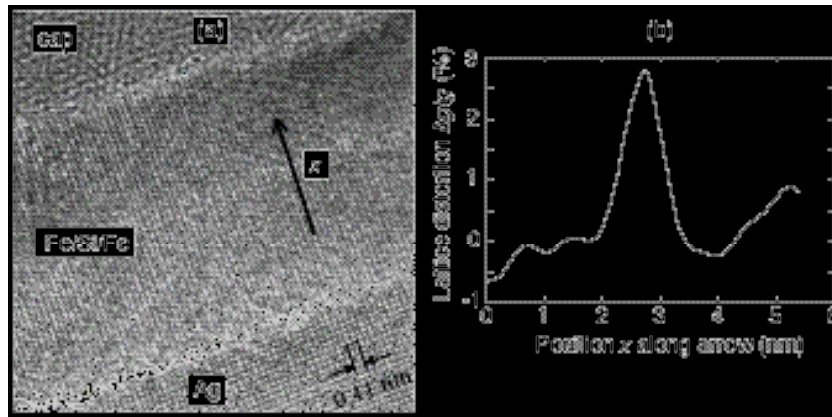

Fig. 2. (a) TEM image of a Fe/Si/Fe trilayer grown on Ag(001) (bottom right) and capped with a ZnS protection layer (top left). (b) Vertical lattice distortion $\Delta g/g$ along the arrow in (a), where g is the vertical separation of the atomic planes in the Fe layers

Epitaxy is further confirmed by the TEM picture in Fig. 2(a), where it is indeed difficult to distinguish the Fe layers and the Si interlayer, because the atomic lattices match almost perfectly. A Fourier transform analysis of the vertical lattice distortion $\Delta g/g$ along the arrow in Fig. 2(a) reveals a difference of about 3% between the Fe layers and the Si interlayer [Fig. 2 (b)]. The fact that the Si interlayer is vertically expanded with respect to the Fe lattice directly

excludes that the Si grows in a tetragonally distorted bulk structure, because the in-plane expansion of the diamond lattice due to the slightly larger Fe(001) lattice would result in a vertical contraction of the order of 9% instead of an expansion by 3%. Therefore, the interlayer adopts a metastable, epitaxially stabilized structure, for which intermixing with Fe cannot be excluded solely based on the TEM data.

3.2. Thickness dependence

The thickness dependence of the bilinear coupling strength J_1 of a Fe(50 Å)/Si(8-20 Å)/ Fe (50 Å) trilayer is shown in Fig. 3. $|J_1|$ decays exponentially with t with a decay length of about 3 Å. For $t \approx 20$ Å the coupling strength decreases to $|J_1| \approx 0.1$ mJ/m². The zero-field antiparallel alignment is observed in the whole range of temperatures and for all spacer

Fig. 3. Bilinear coupling constant J_1 of a Fe (50 Å)/Si(t)/Fe(50 Å) structure *versus* spacer thickness t measured at RT. The fitted curve yields a decay length of 3.3 Å. Inset: Experimental and fitted longitudinal MOKE hysteresis curves for $t = 17.3$ Å clearly show antiparallel alignment (arrows) due to AFC and yield $J_1 = 0.27$ mJ/m²
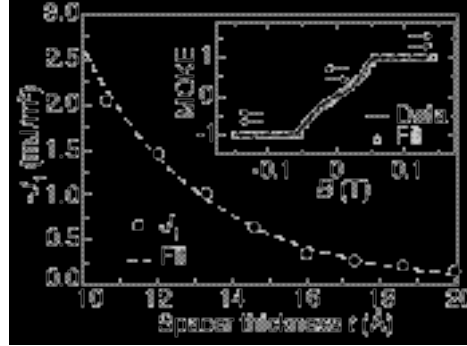
thicknesses. A typical experimental MOKE loop for a Si thickness of 17.3 Å (black) is shown in the inset of Fig. 3 together with the fit (grey circles) that yields antiparallel alignment at zero field (see arrows) due to a bilinear coupling strength of $J_1 = 0.27$ mJ/m².

3.3. Temperature dependence

Figure 4 shows the temperature dependence of the coupling across a Si spacer of 10 Å thickness yielding moderate coupling strength at RT. The Fe layer thickness of 100 Å is larger than our standard value to facilitate the analysis of the SQUID data. Magnetization loops measured by SQUID are fitted using the scheme described in Ref. [14], which takes into account the possibility of a twisted magnetization state due to the strong AFC and,

Fig. 4. Bilinear and biquadratic coupling constants J_1 and J_2 of a Fe(100 Å)/Si(10 Å)/Fe(100 Å) structure *versus* temperature T. The values are derived from fitting SQUID magnetization loops. The solid grey line is the temperature dependence of J_1 predicted by the quantum interference model [Eq. (2)] for insulating spacers
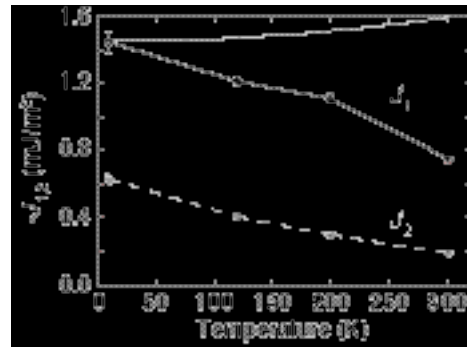
thus, allows for an unequivocal separation and precise determination of J_1 and J_2. The independently, but for the same sample measured temperature dependence of the magnetization is also taken into account. The saturation magnetization drops from 10 to 300 K by about 20%. Both coupling parameters almost linearly decrease with increasing temperature. J_1 decreases from 10 to 300 K by almost 50% and J_2 by about 70%. This temperature dependence is of the same order of magnitude than what we have found previously [7] for metallic $Fe_{50}Si_{50}$ spacer layers. There, the total coupling at the second oscillation maximum, which is dominated by bilinear coupling, decreases from 80 to 300 K by about 45% (again taking into account a drop of the saturation magnetization by about 20%) and levels off below 80 K. The grey solid line in Fig. 4 is the prediction of the quantum interference model for insulating spacers [3] and will be discussed in Sect. 4.

3.4. Transport measurements

First Rowell criterion: In Fig. 5(b) we show the resistance times area product *RA versus t* on a semi-logarithmic scale. The value of *RA* increases at RT strongly with *t* by more than 4 orders of magnitude, while *t* only approximately doubles. The characteristic length t_0 of the order of 1 Å [dashed line in Fig. 5(b)] is significantly shorter compared to previously reported values for structures with amorphous Si spacers [17]. Note, that the coupling strength in Fig. 3 decays with a decay length of the same order of magnitude as the tunneling conductivity.
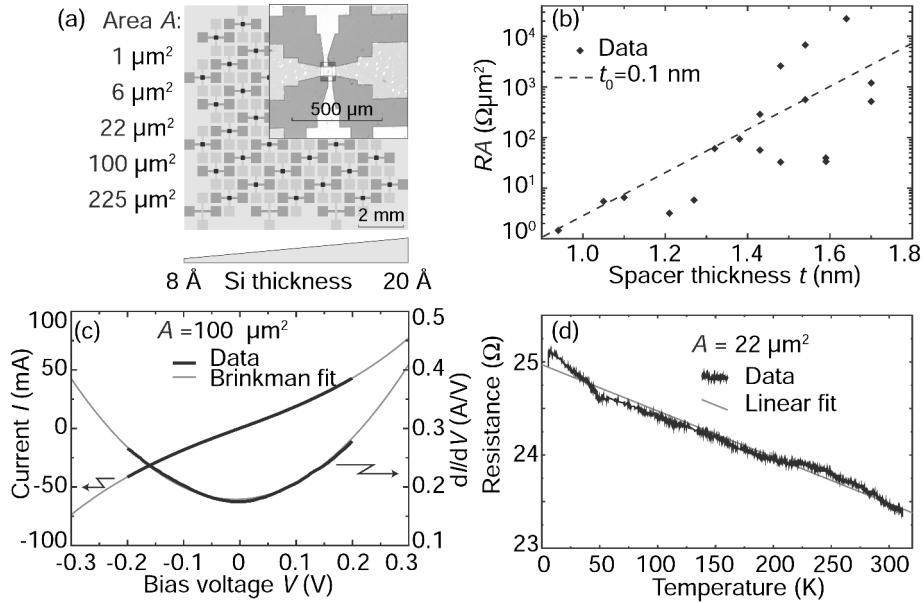
Fig. 5. (a) Layout of the sample for CPP transport measurements. The Si spacer thickness *t* varies along the horizontal axis and the junction size *A* along the vertical axis. The inset shows a photograph of a patterned junction with the contact leads (white and light grey). (b) Dependence of the resistance times area product *RA* on the nominal spacer thickness *t* obtained from Fe(50 Å)/Si(t)/Fe(50 Å) junctions with areas *A* between 22 and 225 μm^2. The dashed line corresponds to a characteristic length $t_0 = 1$ Å. (c) Measured (black) and fitted (grey) *I-V* and *dI/dV-V* curves of a Fe/Si/Fe junction with *A* = 100 μm^2 and *t* = 15.4 Å. (d) Dependence of the resistance on temperature for a Fe/Si/Fe junction with *A* = 22 μm^2 and *t* = 17.0 Å. The solid line is a linear fit that yields a temperature coefficient of -5×10^3 ΩK^1

Second Rowell criterion: A representative *I-V* curve taken at RT and the corresponding *dI/dV-V* curve are presented in Fig. 5(c). They show the typical tunneling-type behavior. The *dI/dV-V* curve is parabolic with its minimum away from *V* = 0. These features are characteristic for tunnel junctions with asymmetric barriers and indicate different conditions at the diffused Fe/Si and Si/Fe interfaces [6, 8, 18]. There is no evidence for a conductivity anomaly near *V* = 0, as previously reported for ferromagnetic junctions with Al-oxide spacers and related to inelastic scattering assisted by magnons and impurities [19]. Similar *I-V* curves can occur when transport is due to another conductivity channel, namely submicron-sized pinholes, which can mimic elastic tunneling [11]. As we will show below based on an analysis of the temperature dependence of the resistance, this metallic-type channel gives here no significant contribution. We observe tunneling-type *I-V* curves only for *t* > 15 Å, where the voltage drop is sufficient to reveal the non-linear part of *I-V* characteristics. The barrier heights ø derived from Brinkman fits [20] vary from 0.3 to 0.8 eV for different junctions, which all show a definite barrier asymmetry Δø in the range from 0.1 to 0.3 eV. Explicit Brinkman fit results for a series of different junctions and a detailed discussion can be found in Ref. [13].

Third Rowell criterion: A typical temperature dependence of the zero-bias resistance is presented in Fig. 5(d). The resistance slightly decreases with temperature and, thus, shows tunneling-type behavior. The total change of resistance from 4 K to RT does not exceed 5-7%. We relate the change of resistance to prevailing direct elastic tunneling, which yields only weak temperature dependence due to the broadening of Fermi distributions. The elastic but resonant tunneling channel is much weaker than the direct one and obeys a decay length, which is twice as large as the decay length of direct tunneling. However, resonant elastic tunneling cannot definitely be excluded for our junctions with *t* lying in the narrow interval between 14 and 17 Å. Different weights of the contributions from elastic direct and elastic resonant tunneling could lead to the scattering of the *RA* values in Fig. 5(b). Next, we consider inelastic tunneling based on thermo-activated hopping across impurity states in the barrier. For this channel a strong decrease of resistance with temperature is expected [17]. Thus, this channel is not dominant in our junctions.

4. DISCUSSION

The transport measurements show that epitaxial, AF-coupled Fe/Si/Fe junctions fulfill all three necessary and sufficient Rowell criteria for direct elastic electron tunneling. A significant metallic contribution to the electron transport through pinholes can be excluded. The experimentally proven coexistence of strong AFC and electron transport *via* direct tunneling across nominally pure Si spacers proves that a non-conducting interlayer mediates the AF exchange coupling. The underlying, presumably so far disregarded coupling mechanism gives

rise to a rather strong interaction, as the observed coupling strengths are among the largest ever reported – including metal spacers [2] – and clearly exceed the corresponding values for amorphous Si spacers by 3 orders of magnitude [21]. In the case of nominally pure Si spacers, the coupling also exceeds the values previously found for various Fe/Fe$_{1-x}$Si$_x$/Fe structures [6, 7, 22-24].

Hunziker and Landolt [25] proposed a heat-induced coupling mechanism to explain the interlayer coupling across amorphous semiconductor spacers (*a*-Si, *a*-Ge, *a*-ZnSe), which is based on the interaction of localized, weakly bound states at the interfaces. These states are assumed to originate from impurities in the semiconductor material. They overlap in the spacer to form large molecular orbitals, for which the Pauli principle requires a different energy for the parallel and antiparallel spin configurations. This difference determines the coupling strength. A key feature of this mechanism is a strong positive temperature coefficient, which arises from the thermal population of these orbitals. For our epitaxial system, the transport measurements and the negative temperature coefficient in Fig. 4 negate heat-induced effects. Furthermore, a rather high density of impurities of the order of 10^{19} cm^{-3} must be assumed to obtain a 10^3 times stronger coupling than in Ref. [25]. Therefore, we dismiss this mechanism for epitaxial Fe/Si/Fe trilayers.

Another coupling mechanism for insulating spacers was derived by Bruno [3, 4] who extended the quantum interference model to insulating materials by introducing the concept of complex Fermi surfaces. Here, the coupling arises from spin-dependent interferences of electron waves – Bloch waves for metals and evanescent waves for insulators – in the spacer, which result from spin-dependent reflections at the interfaces. The model predicts for insulating (metallic) spacers a positive (negative) temperature coefficient, in both cases due to the thermal smearing of the Fermi surface. For metals the fuzzyness of the Fermi surface affects the interference condition, and for insulators states above the Fermi level experience a lower tunneling barrier and, thus, have a higher transmission probability. The temperature dependence of J_1 for an insulating spacer is given by [3, 4]

$$J_1(T) = J_1(0) \frac{T/T_0}{\sin\left(T/T_0\right)} \,, \tag{2}$$

where T_0 is of the order of 200-600 K for barrier heights of 0.1-0.9 eV [3, 4]. Therefore, the coupling is almost constant below 300 K as demonstrated by the solid grey line in Fig. 4 which is calculated for $T_0 = 400$ K corresponding to a barrier height of about 0.4 eV and normalized to the experimental J_1 value at 10 K. The experimental decrease of J_1 in Fig. 4 is in disagreement with the prediction of Eq. (2). Nevertheless, we consider the $T = 0$ limit, where Bruno's model reduces to Slonczewski's spin-current model [26], in order to compare the thickness dependences of experiment and model. Using a two-band approximation for the exchange-split ferromagnet, the coupling strength is given by [26]

$$J_1 = \frac{(U - E_\mathrm{F})}{8\pi^2 t^2} \frac{8k^3 \left(k^2 - k_\uparrow k_\downarrow\right) \left(k_\uparrow - k_\downarrow\right)^2 \left(k_\uparrow + k_\downarrow\right)}{\left(k^2 + k_\uparrow^2\right)^2 \left(k^2 + k_\downarrow^2\right)^2} e^{-2kt} \,, \tag{3}$$

where ($U - E_F$) is the barrier height, $k_{\uparrow(\downarrow)}$ the Fermi wave vectors for the spin up (down) bands of the ferromagnet, and $k^2 = 8\pi^2 m_{eff}(U - E_F)/h^2$ with m_{eff} the effective electron mass in the interlayer. This equation was employed by Faure-Vincent *et al.* [5] to successfully fit the strength and thickness dependence of the AF coupling in epitaxial Fe/MgO/Fe structures. If we apply the same procedure with the same parameters ($k_\uparrow = 1.09$ Å^1 and $k_\downarrow = 0.43$ Å^1 after Ref. [27]) to our data, then we get curves similar to the dashed line in Fig. 3, but the fitted values for the barrier height and the effective mass are physically not meaningful, *e.g.* several keV for ($U - E_F$) and 10^5 rest masses for m_{eff}. The reason is the strong coupling which requires in Eq. (3) a large prefactor [*i.e.* a huge barrier height ($U - E_F$)]. On the other hand, the decay length in the exponent of Eq. (3) given by k must be of the order of a few Å and, thus, forces m_{eff} to be extremely small to compensate the huge ($U - E_F$). In other words, the quantum interference or spin-current model, respectively, in the two-band approximation as the basis of Eq. (3) can for Fe/Si/Fe – in contrast to Fe/MgO/Fe in Ref. [5] – not at all account for the observed AF coupling.

5. CONCLUSIONS

The very strong antiferromagnetic interlayer exchange coupling in epitaxial Fe/Si/Fe(001) trilayers is mediated by a non-conductive Si spacer layer that acts in CPP transport measurements as a tunneling barrier with a height of several tenths of an eV. The temperature dependence of the bilinear coupling constant determined taking into account the experimental temperature dependence of the saturation magnetization reveals a negative temperature coefficient. This behavior and the strength of the coupling are not compatible with the molecular-orbital model of heat-induced exchange coupling proposed for amorphous semiconductor spacer [25]. The quantum interference model [3, 4, 26] predicts the observed thickness dependence and for our circumstances (*i.e.* barrier height) a rather weak positive temperature dependence. However, the present data about the temperature dependence of a moderately coupled Fe(100 Å)/Si(10 Å)/Fe(100 Å) trilayer is not compatible with this prediction. Furthermore, the model in the simple two-band approximation for the ferromagnet and a "free-electron-like" tunneling behavior in the spacer completely fails to predict the observed coupling strength by at least one order of magnitude. The understanding of the mechanism for the strong antiferromagnetic coupling across epitaxial, highly resistive Si spacers still remains an open question.

References

[1] P. Grünberg, R. Schreiber, Y. Pang, M. B. Brodsky, and H. Sowers, Phys. Rev. Lett. **57**, 2442 (1986).
[2] D. E. Bürgler, P. Grünberg, S. O. Demokritov, and M. T. Johnson, in *Handbook of Magnetic Materials*, vol. **13** ed. by K. H. J. Buschow (Elsevier, 2001).
[3] P. Bruno, Phys. Rev. B **52**, 411 (1995).
[4] P. Bruno, J. Appl. Phys. **76**, 6972 (1994).
[5] J. Faure-Vincent, C. Tiusan, C. Bellouard, E. Popova, M. Hehn, F. Montaigne, and A. Schuhl, Phys. Rev. Lett. **89**, 107206 (2002).
[6] R. R. Gareev, D. E. Bürgler, M. Buchmeier, R. Schreiber, and P. Grünberg, J. Magn. Magn. Mater. **240**, 235 (2002).

 [7] R. R. Gareev, D. E. Bürgler, M. Buchmeier, D. Olligs, R. Schreiber, and P. Grünberg, Phys. Rev. Lett. **87**, 157202 (2001).
 [8] R. R. Gareev, D. E. Bürgler, M. Buchmeier, R. Schreiber, and P. Grünberg, Appl. Phys. Lett. **81**, 1264 (2002).
 [9] R. R. Gareev, D. E. Bürgler, M. Buchmeier, R. Schreiber, and P. Grünberg, Trans. Magn. Soc. Jpn., **2,** 205 (2002).
[10] R. R. Gareev, D. E. Bürgler, R. Schreiber, H. Braak, M. Buchmeier, and P. A. Grünberg, Appl. Phys. Lett. **83**, 1806 (2003).
[11] D. A. Rabson, B. J. Jönsson-Åkerman, A. H. Romero, R. Escudero, C. Leighton, S. Kim, and I. K. Schuller, J. Appl. Phys. **89**, 2786 (2001).
[12] J. J. Åkerman, R. Escudero, C. Leighton, S. Kim, D. A. Rabson, R. W. Dave, J. M. Slaughter, and I.K. Schuller, J. Magn. Magn. Mater. **240**, 86 (2002).
[13] R. R. Gareev, L. L. Pohlmann, S. Stein, D. E. Bürgler, and P. A. Grünberg, J. Appl. Phys. **93**, 8038 (2003).
[14] M. Buchmeier, B. K. Kuanr, R. R. Gareev, D. E. Bürgler, and P. Grünberg, Phys. Rev. B **67**, 184404 (2003).
[15] C.L. Jia, M. Lentzen, and K. Urban, Science **299**, 870 (2003).
[16] R. J. M. van de Veerdonk, J. Novak, R. Meservey, J. S. Moodera, and W. J. M. de Jonge, Appl. Phys. Lett. **71**, 2839 (1997).
[17] Y. Xu, D. Ephron, and M.R. Beasley, Phys. Rev. B **52**, 2843 (1995).
[18] R. Kläsges, C. Carbone, W. Eberhardt, C. Pampuch, O. Rader, T. Kachel, and W. Gudat, Phys. Rev. B **56**, 10801 (1997).
[19] J. S. Moodera and G. Mathon, J. Magn. Magn. Mater. **200**, 248 (1999).
[20] W. F. Brinkman, R. C. Dynes, and J. M. Rowell, J. Appl. Phys. **41**, 1915 (1970).
[21] B. Briner and M. Landolt, Phys. Rev. Lett. **73**, 340 (1994).
[22] Y. Endo, O. Kitakami, and Y. Shimada, J. Appl. Phys. **87**, 6836 (2000).
[23] E. E. Fullerton, J. E. Mattson, S. R. Lee, C. H. Sowers, Y. Y. Huang, G. Felcher, S. D. Bader, and F.T. Parker, J. Magn. Magn. Mater. **117**, L301 (1992).
[24] J. J. de Vries, J. Kohlhepp, F. J. A. den Broeder, R. Coehoorn, R. Jungblut, A. Reinders, and W.J.M. de Jonge, Phys. Rev. Lett. **78**, 3023 (1997).
[25] M. Hunziker and M. Landolt, Phys. Rev. Lett. **84**, 4713 (2000).
[26] J. C. Slonczewski, Phys. Rev. B **39**, 6995 (1989).
[27] V. Moruzzi, *Calculated Electronic Properties of Transition Metal Alloys* (World Scientific, Singapore, 1994).